Phonon traces in glassy vibrations

N. S. Shcheblanov [1,2,3,*] M. E. Povarnitsyn [4,5,†] J. D. Wiles,[6] S. R. Elliott,[7] and S. N. Taraskin [7,8]

[1]*Université Paris-Est, Laboratoire NAVIER (UMR 8205), CNRS, ENPC, IFSTTAR, F-77420 Marne-la-Vallée, France*
[2]*Laboratoire des Solides Irradiés CEA-CNRS, École Polytechnique, F-91128 Palaiseau, France*
[3]*Centre de Physique Théorique, CNRS, École Polytechnique, F-91128 Palaiseau, France*
[4]*Moscow Institute of Physics and Technology, Institutsky Lane 9, Dolgoprudny, Moscow Region 141700, Russia*
[5]*Joint Institute for High Temperatures, RAS, 13 Building 2 Izhorskaya Street, Moscow 125412, Russia*
[6]*Cavendish Laboratory, University of Cambridge, Cambridge CB3 0HE, United Kingdom*
[7]*Department of Chemistry, University of Cambridge, Cambridge CB2 1EW, United Kingdom*
[8]*St. Catharine's College, University of Cambridge, Cambridge CB2 1RL, United Kingdom*

A numerical approach, based on a local comparative projectional analysis onto symmetry modes of elementary structural units of glasses and their crystalline counterparts, is developed and used for the analysis of atomic vibrations in glasses in terms of phonons for the entire frequency range. The results of such an analysis shed light on the origin of the modes in the controversial low-frequency range, including the boson-peak region. Comparative analyses undertaken for glass, lattice-glass, and polycrystalline models reveal the role of different types of disorder in atomic vibrations.

I. INTRODUCTION

The idea of similarities between atomic vibrations in crystals (phonons) and in glasses has been around for decades [1–6]. If an arbitrary crystalline lattice is slightly perturbed, e.g., by introducing atomic defects, then atomic vibrations can still be approximately expressed in terms of phonons [7,8]. In network glasses, crystalline order is lost but the short and midrange order survives in the form of the same atomic structural building blocks (units) present both in glasses and in corresponding crystals so that the vibrational motion of those might share some similarity. In the absence of a direct comparative analysis of vibrations in glasses and crystals, the following general questions remained unclear: (i) Do glassy vibrations in different frequency ranges resemble (originate from) phonons in corresponding crystals? (ii) If yes, then what are their frequency-frequency *correlations*, and what are the typical length scales on which the vibrations are similar? (iii) What is the role of different types of disorder in the formation of the vibrational spectrum of glasses? A particular question about the origin of the low-frequency boson-peak (BP) modes in glasses [2,3,9,10] could benefit from such a comparative analysis as well.

In this paper, we address all the above questions. For the question about the nature and origin of vibrational eigenmodes in disordered solids throughout the whole frequency range, our main findings demonstrate clear frequency-frequency correlations for vibrations of local structural units in glasses and corresponding crystals in different parts of the vibrational spectrum and, thus, reveal phonon traces in

the glassy modes. In particular, we give further evidence in support of the viewpoint relating the BP modes with strongly hybridized and pushed-down-in-frequency phonons present in crystalline counterparts [3,10], thus complementing some alternative scenarios for the nature of the BP [9,11–17]. These results have been obtained using an approach for the comparison of atomic vibrations in glassy, lattice-glass, polycrystalline models, and their crystalline counterparts, by means of the projection of local atomic vibrations onto symmetry modes characteristic of structural units.

The paper is structured as follows. In Sec. II, we discuss the structural models used in the analysis by a comparative symmetry-mode projection technique outlined in Sec. III. The results are presented in Sec. IV, and conclusions are given in Sec. V.
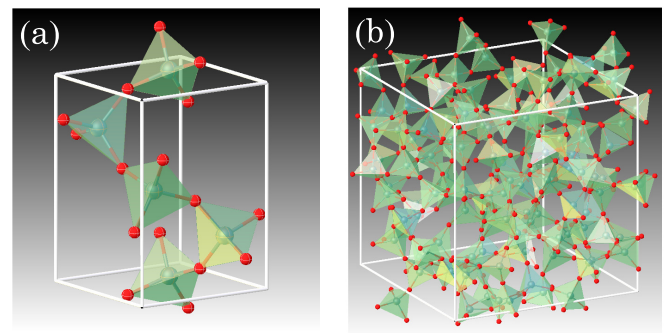

FIG. 1. (a) Unit cell of the α-cristobalite phase of SiO_2 containing four tetrahedral structural units. (b) The corner-shared tetrahedral network of a v-SiO_2 glass model. Oxygen and silicon atoms are depicted by red and green colors, respectively. Only 648 atoms are displayed in (b) for clarity of presentation.
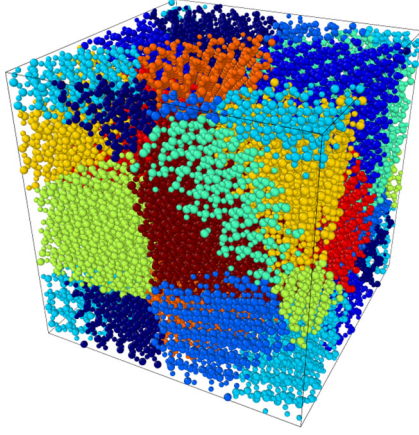
*n.s.shcheblanov@gmail.com
†povarnitsyn.me@mipt.ru

024202-1

FIG. 2. Structural model of polycrystalline silica (pc-SiO$_2$) consisting of 25 637 atoms in ten α-cristobalite grains shown by different colors.

II. STRUCTURAL MODELS

Our approach is illustrated by an analysis of vibrations in large structural models of a prototype glass, vitreous silica (v-SiO$_2$), as well as a lattice-glass (lg-SiO$_2$), polycrystalline silica (pc-SiO$_2$), and their crystalline counterpart α-cristobalite [1,10,18,19]. Structural models of v-SiO$_2$ (24 000 atoms) and α-cristobalite were produced by means of classical molecular-dynamics simulations (LAMMPS package [20]), using the van Beest, Kramer, and van Santen potential [21] with Wolf's cutoff for Coulombic interactions [22,23] (see Fig. 1 and the Supplemental Material [24]). In order to prepare an α-cristobalite model, we varied the elementary cell size to obtain the phonon band structure most similar to that found by recent *ab initio* simulations [25]. Parameters of the α- and β-cristobalite unit cells used in simulation and found experimentally [26,27] are presented in the Supplemental Material [24].

The models of lg-SiO$_2$ were constructed by the rigid rotation of bridging O atoms in α-cristobalite about the axis connecting two Si atoms forming a bridge by a random angle θ normally distributed around zero mean, corresponding to equilibrium positions of O atoms with a standard deviation of $\sigma_\theta = 15°$. For this value of σ_θ, the distribution of the shapes of tetrahedra characterized by the tetrahedral order parameter $q = 1 - 3/8 \sum_{i=1}^{6} [\cos(\psi_i) + 1/3]^2$ (where ψ_i is an angle formed by two vectors pointing from a Si atom to two of its nearest O neighbors, and the sum is taken over all distinct pairs of O neighbors [28]) in v-SiO$_2$ and lg-SiO$_2$ are sufficiently similar with $q \simeq 0.982 \pm 0.015$ and $q \simeq 0.979 \pm 0.016$, respectively.

A polycrystalline model (see Fig. 2) consisting of 25 637 atoms was obtained by matching ten grains of α-cristobalite each containing approximately 200 unit cells. Some of the unit cells in the crossover (amorphous) regions between grains were cut under the constraint that the minimal Si-O distance is not less than 1.5 Å. The model of pc-SiO$_2$ was created by using the ATOMSK program [29].

Both crystalline and glassy SiO$_2$ structures can be described as networks of corner-shared tetrahedra XY$_4$ or molecular units XY$_2$ (see Fig. 1). The XY$_4$ tetrahedron and
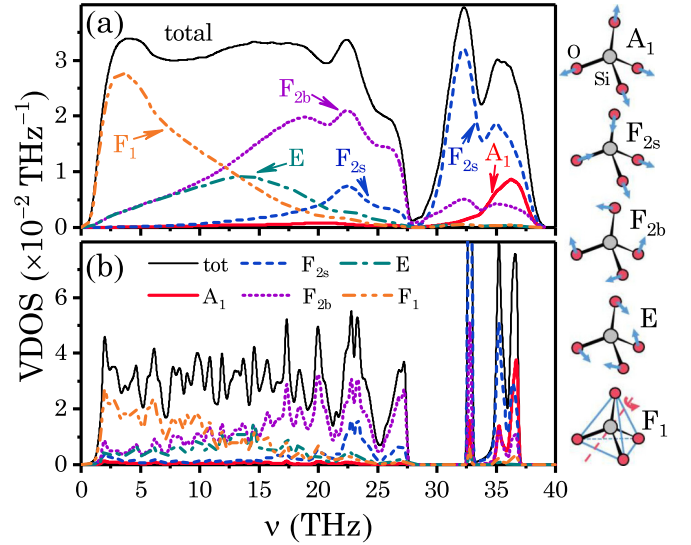

FIG. 3. (a) The partial vibrational density of states (VDOS) for the T_d-symmetry modes of SiO$_4$ units: A_1 symmetric stretching (solid red line), F_{2s} asymmetric stretching (dashed blue line), F_{2b} bending (dotted magenta line), E bending (dot-dashed green line), F_1 solid-unit rotations (double dot-dashed orange line), and total VDOS (black solid line) for v-SiO$_2$. (b) The partial VDOS of α-cristobalite with the same color code as in panel (a). The right vertical column displays tetrahedral structural units with the blue arrows showing the relative motion of O atoms for the T_d group. The dashed red line in the lowest tetrahedron represents the axis of rotation shown by the red arrow.

the symmetric XY$_2$ molecule belong to the cubic T_d and orthorhombic C_{2v} point groups, respectively.

III. COMPARATIVE SYMMETRY-MODE PROJECTION TECHNIQUE

The local atomic vibrations of these structural units can be characterized by complete orthonormal sets $\{\mathbf{A}^{(d)}\}$ ($d = 1, \ldots, d_M$) of 6,

$$\mathbf{A}^{(d)} \in \left\{ \mathbf{S}^{(A_1)}, \mathbf{S}^{(B_1)}, \mathbf{B}^{(A_1)}, \mathbf{R}_{1-3}^{(B_2)} \right\},$$

and 12,

$$\mathbf{A}^{(d)} \in \left\{ \mathbf{S}^{(A_1)}, \mathbf{S}_{1-3}^{(F_2)}, \mathbf{B}_{1-3}^{(F_2)}, \mathbf{B}_{1-2}^{(E)}, \mathbf{R}_{1-3}^{(F_1)} \right\},$$

symmetry modes belonging to the C_{2v}- and T_d-symmetry groups, respectively, see the Supplemental Material [24] and Refs. [30,31]. In a local projectional analysis, the nth vibrational eigenvectors for v-SiO$_2$ and α-cristobalite (instantaneous normal modes for lg-SiO$_2$ and pc-SiO$_2$ [32]) are split into the local relative displacement vectors $\mathbf{u}_{i(i')}^n$ describing the motion of atoms i' within the structural unit i and expanded in the symmetry-mode basis. The coefficients in such an expansion represent the components of a d_M-dimensional position vector,

$$\mathbf{g}_i^n = \left\{ \mathbf{u}_i^n \cdot \mathbf{A}_i^{(d)} \right\}, \quad \text{with } d = 1, \ldots, d_M, \qquad (1)$$

in symmetry-mode space. Their squared magnitudes averaged over all structural units are used for the local symmetry-mode assignment both for silica [30,31,33,34] and for α-cristobalite
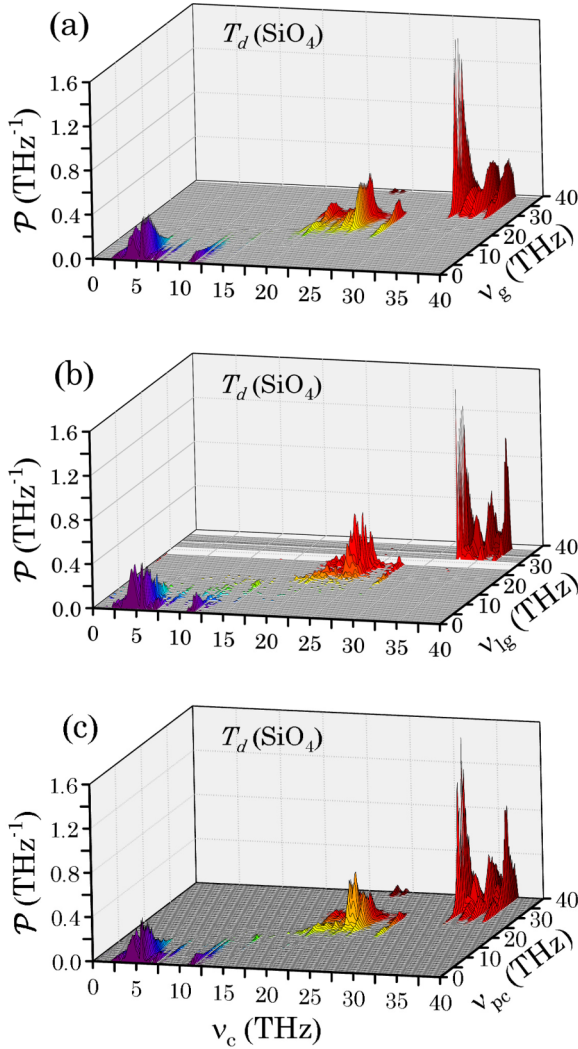
FIG. 4. Correlation function $\mathcal{P}(\nu_\mu, \nu_c)$ [see Eq. (6)] with $\varepsilon = 0.95$ [see Eq. (3)] for the local vibrations of the T_d group in (a) v-SiO$_2$, (b) lg-SiO$_2$ with $\sigma_\theta = 15°$, and (c) pc-SiO$_2$.

and which show clear correlations in the symmetry of local vibrations in v-SiO$_2$ and α-cristobalite through the entire frequency range [cf. Figs. 3(a) and 3(b)]. However, the local projectional analysis itself does not provide a direct comparison of glassy eigenmodes with phonons.

Below, we develop this framework enabling us to perform a comparative analysis of glassy and crystalline modes within the following qualitative idea. Vibrations of an arbitrary structural unit for any glassy (crystalline) mode can be projected onto symmetry modes for that unit and, thus, characterized by a *glassy* (*phonon*) position vector. The closeness between glassy and phonon vectors can be assessed by means of their cosine similarity which is used in the *correlation* function characterizing the similarity between *entire* glassy and crystalline modes.

The comparative analysis begins by defining a "projector" $\mathcal{P}_{i_\mu,i_c}^{n_\mu,n_c}$ for unit-vectors $\hat{\mathbf{g}}_{i_\mu,m_\mu}^{n_\mu}$ and $\hat{\mathbf{g}}_{i_c,m_c}^{n_c}$ which describe the structural units i_μ and i_c for a glassy eigenmode n_μ ($\mu =$
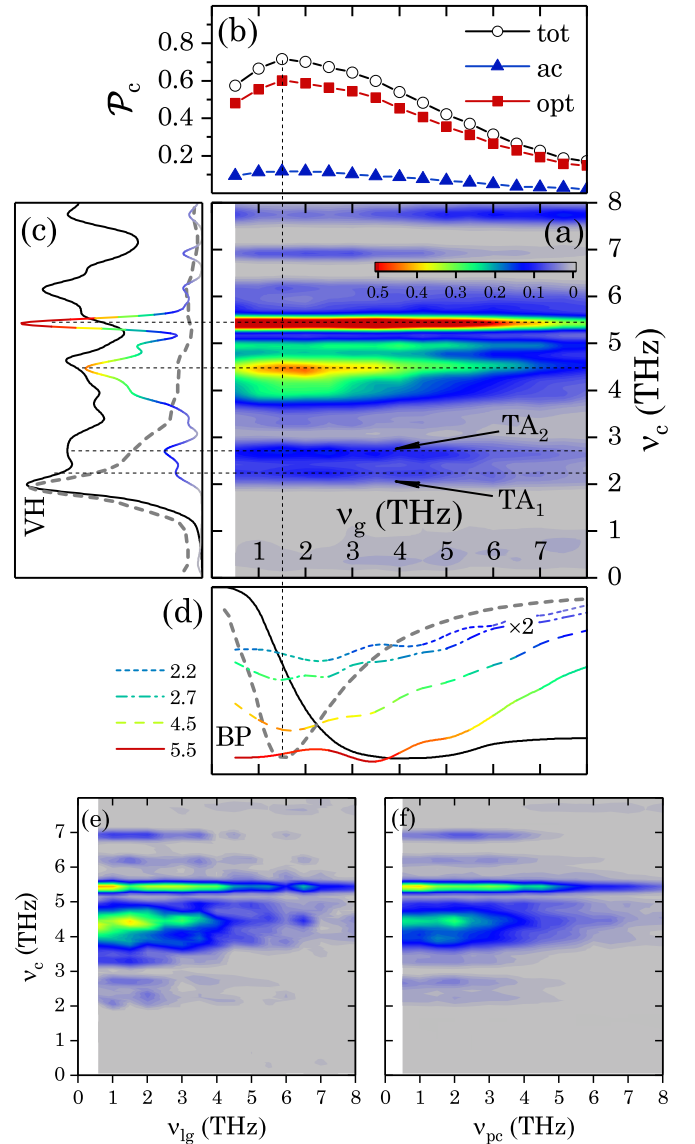

FIG. 5. (a) Correlation function $\mathcal{P}(\nu_g, \nu_c)$ for the local vibrations of the T_d group in v-SiO$_2$. The arrows TA$_{1,2}$ indicate the contributions of transverse-acoustic van Hove (VH) modes. (b) Crystallinity $\mathcal{P}_c(\nu_g)$ [see Eq. (5)] of glassy modes (black curve with empty circles) vs ν_g and its split into acoustic [(ac), $\beta = 1, 2, 3$] and optic [(opt), $\beta = 4, \ldots, 36$] contributions. (c) Projection slice of the correlation function (multicolored curve) at $\nu_g \simeq 1.5$ THz. (d) Slices of the correlation function at $\nu_c \simeq 2.2, 2.7, 4.5$, and 5.5 THz (multicolored curves). The slices at $\nu_c = 2.2$ and 2.7 THz are multiplied by a factor of 2 for better display. The total and reduced VDOS of α-cristobalite and v-SiO$_2$ are shown in panels (c) and (d) by solid black and dashed gray curves, respectively. Panels (e) and (f) display $\mathcal{P}(\nu_\mu, \nu_c)$ for the local vibrations of the T_d group in lg-SiO$_2$ and pc-SiO$_2$, respectively.

g, lg, pc) and a phonon n_c, respectively, i.e.,

$$\mathcal{P}_{i_\mu,i_c}^{n_\mu,n_c} = \max_{m_{\mu,c}} \left\{ \left| \hat{\mathbf{g}}_{i_\mu,m_\mu}^{n_\mu} \cdot \hat{\mathbf{g}}_{i_c,m_c}^{n_c} \right| \right\}. \quad (2)$$

The index $m_{\mu,c} \in \mathcal{M}$ with $\mathcal{M}$ being the set of 2 and 12 permutations of the atoms within the XY$_2$ and XY$_4$ glassy (crystalline) structural units (see the Supplemental Material [24] for more details). We aim to find the crystalline eigen-
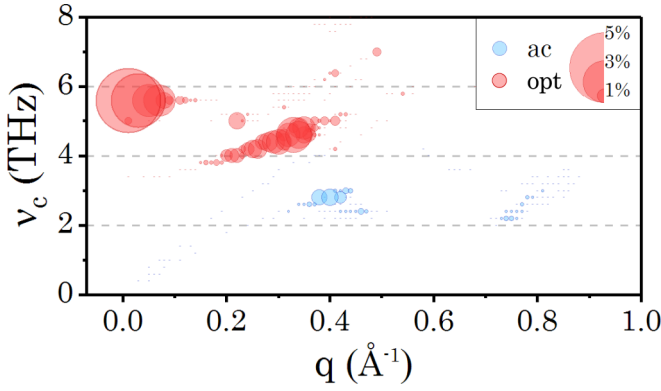
FIG. 6. Crystallinity decomposition showing the percentage of tetrahedra (T_d group, $\varepsilon = 0.95$) in the glassy mode with $\nu_g \simeq 1.5$ THz correlated with phonons of a particular frequency ν_c and wave-vector magnitude $|\mathbf{q}|$. Contributions from acoustic ($\beta = 1, 2, 3$) and optic ($\beta = 4, \ldots, 36$) phonons are shown by blue and red circles, respectively.

modes which most resemble a given glassy mode, and, thus, we define the binary projector $\hat{\mathcal{P}}_{i_\mu}[\nu_\mu, (\beta\mathbf{q})_{\max}]$, which is related to the maximum value (among all possible crystalline modes and units) of the projector given by Eq. (2), i.e.,

$$\hat{\mathcal{P}}_{i_\mu}[\nu_\mu, (\beta\mathbf{q})] = \begin{cases} 1, & \text{if } \varepsilon < \max_{n_c, i_c}\left\{\mathcal{P}_{i_\mu, i_c}^{n_\mu, n_c}\right\} \leqslant 1, \\ 0, & \text{otherwise,} \end{cases} \quad (3)$$

where ε is the close-to-unity tolerance parameter, ν_μ stands for the frequency of the glassy eigenmode n_μ, and $(\beta\mathbf{q})$ describes a phonon with a frequency $\nu_c \equiv \nu_\beta(\mathbf{q})$ for which the maximum value of $\mathcal{P}_{i_\mu, i_c}^{n_\mu, n_c}$ is achieved, i.e., $(\beta\mathbf{q}) \equiv (\beta\mathbf{q})_{\max}$. The binary projector given by Eq. (3) counts the pairs of structural units in glass and crystal for which the vibrations are similar, i.e., the *distance* between glassy and phonon symmetry vectors is relatively short. Several glassy units can contribute to the same phonon and, thus, the quantity $\mathcal{P}[\nu_\mu, (\beta\mathbf{q})]$ averaged over all glassy units,

$$\mathcal{P}[\nu_\mu, (\beta\mathbf{q})] = \frac{1}{N_\mu}\sum_{i_\mu}\hat{\mathcal{P}}_{i_\mu}[\nu_\mu, (\beta\mathbf{q})] \quad (4)$$

represents the discrete distribution over the phonon spectrum of the similarity parameter, called *crystallinity*. For a given point $\mathbf{q}$ in the Brillouin zone and branch number β, $\mathcal{P}[\nu_\mu, (\beta\mathbf{q})]$ gives the relative number of glassy units in a glassy mode ν_μ which exhibit a local motion similar to that of one of the structural units for this phonon. Finally, integration over all phonons defines the overall crystallinity $\mathcal{P}_c(\nu_\mu)$ of a glassy mode ν_μ,

$$\mathcal{P}_c(\nu_\mu) = \sum_{\beta\mathbf{q}}\mathcal{P}[\nu_\mu, (\beta\mathbf{q})] = \int \mathcal{P}(\nu_\mu, \nu_c)d\nu_c, \quad (5)$$

where we introduce the continuous frequency distribution of crystallinity or frequency-frequency correlation function,

$$\mathcal{P}(\nu_\mu, \nu_c) = \sum_{\beta\mathbf{q}}\mathcal{P}[\nu_\mu, (\beta\mathbf{q})]\delta[\nu_c - \nu_\beta(\mathbf{q})] \quad (6)$$
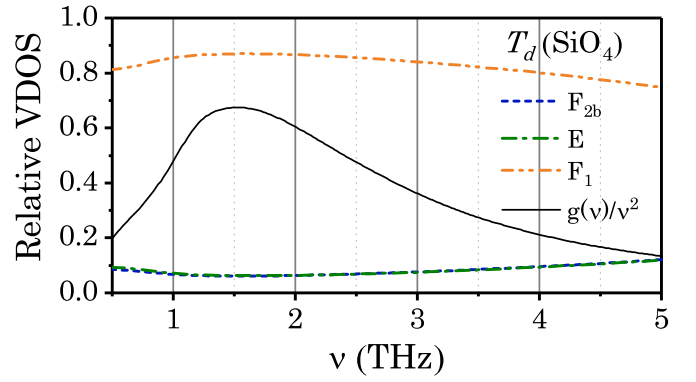

FIG. 7. Relative contributions of T_d-symmetry modes F_{2b} (dashed blue curve), E (dashed-dotted green curve), and F_1 (dashed-dot-dot orange curve) in the VDOS of v-SiO$_2$. The reduced VDOS is schematically shown by the solid black curve.

being a similarity characteristic between a glassy mode ν_μ and phonons with frequency near ν_c.

IV. RESULTS

The results for $\mathcal{P}(\nu_\mu, \nu_c)$ are shown in Fig. 4 for tetrahedral XY$_4$ units (and in Figs. S4(b) and S4(c) of the Supplemental Material [24] for XY$_2$ and YX$_2$ units). For all models, v-SiO$_2$, lg-SiO$_2$, and pc-SiO$_2$, the function $\mathcal{P}(\nu_\mu, \nu_c)$ has the shape of narrow ridges along the glass frequency axis ν_μ, exhibiting peak regions where the glassy (polycrystalline) modes and phonons show a significant similarity. Qualitatively, these findings can be explained by assuming that the disordered material is made from the corresponding crystal by moving and/or deforming the building blocks (e.g., when constructing lg-SiO$_2$ and pc-SiO$_2$). Any motion of building blocks likely destroys the phonon spectrum of the crystal by washing out and shifting the sharp features of the spectrum. The disordered vibrational modes, thus, might result from a mixture (hybridization) of phonons within some typical phonon-phonon interaction frequency scale. The larger this scale, the less similar are glassy modes to some particular phonons. At the phonon-band boundaries, the phonon spectrum transforms to the glassy band tails. These phonon-hybridization effects might be less significant for glassy modes in the tail regions because fewer phonons are involved in mixing, i.e., only the phonons coming from the band producing the tail. In the midband region, this band-edge effect is suppressed, and hybridization effects might be stronger.

Our analysis gives strong evidence in support of such a qualitative picture in v-SiO$_2$, lg-SiO$_2$, and pc-SiO$_2$. The v-SiO$_2$ vibrational spectrum [see Fig. 3(a)] consists of one wide band of width $\simeq 27$ THz and one narrow (with a width of $\simeq 10$ THz) high-frequency band separated by an $\simeq 3$-THz gap (filled by the tail localized states [35]) and can be imagined as originating from the very similar phonon spectrum of α-cristobalite [cf. Figs. 3(a) and 3(b)]. Very clear phonon traces are seen (see Fig. 4 and Fig. S4 in the Supplemental Material [24]) for glassy modes near the bottom ($\nu_\mu \lesssim 10$ THz) and top ($18 \lesssim \nu_\mu \lesssim 28$ THz) of the main wide band and within the entire high-frequency band ($30 \lesssim \nu_\mu \lesssim 40$ THz). A typical
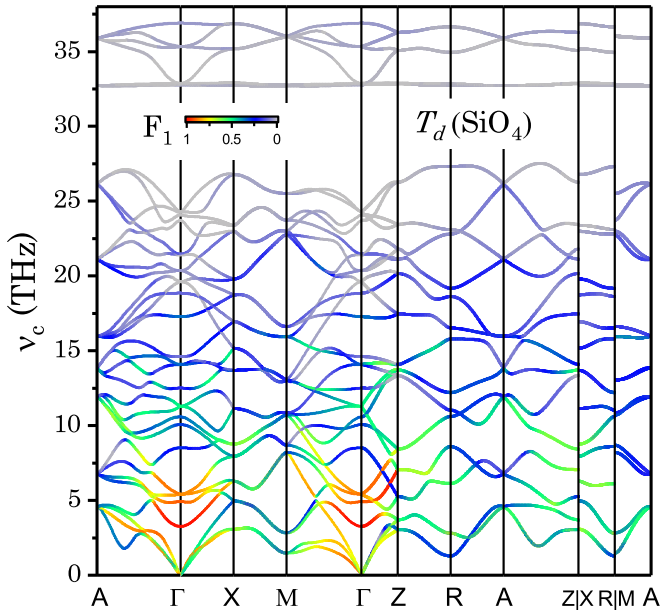
FIG. 8. The phonon dispersion in α-cristobalite, colored according to the relative contribution of the F_1-symmetry mode of the T_d group. The magnitude of the wave vectors at different symmetry points in the Brillouin zone (see Fig. S5 in the Supplemental Material [24] for more details) are the following: $q(\Gamma) = 0$, $q(A) \simeq 1.02$, $q(Z) \simeq 0.5$, $q(X) \simeq 0.6$, and $q(M) \simeq 0.89$ Å^{-1}.

frequency scale for these traces $\Delta\nu \sim 5$ THz along the ν_c axis gives an estimate for the strength of the phonon-phonon interactions. The correlations are especially strong for all types of structural units in the high-frequency band where the vibrational motion has sufficiently local character, evident from low values of the participation ratio (PR) (see Fig. S6 in the Supplemental Material [24]), and dominated by the A_1- and F_{2s}-symmetry modes of the T_d group in v-SiO$_2$, lg-SiO$_2$, pc-SiO$_2$, and α-cristobalite. No noticeable traces are observed in the midband region (10–20 THz). In the low-frequency range, the reconstruction of the phonon spectrum occurs in a peculiar way due to the presence there of acoustic and optic phonons. The optic phonons are hybridized and pushed down the spectrum due to level-repelling effects [3] from the bulk of the band in a similar way as near the top of the band where they are pushed up the spectrum. On the way down the spectrum, the optic phonons can also be hybridized with acoustic phonons when they enter the frequency range of acoustic branches. The acoustic phonons are also mixed between themselves, exhibiting less mixing with decreasing frequency because the long-wavelength acoustic waves are less affected by disorder.

This qualitative scenario is supported by the results of our analysis (see Fig. 5) in the low-frequency domain containing the glassy modes, including the BP modes, the origin of which is highly debated [3,9–14]. It is evident from Fig. 5 that the local vibrations in glassy modes from the BP region ($\simeq 1.5$ THz) are very similar to the local vibrations for phonons of several types. The highest degree of similarity is found for transverse-optic phonons with frequencies at $\simeq 5.5$ THz, indicated by a sharp narrow trace in Fig. 5(a) and by a pronounced peak in the multicolored curve in panel (c).

Slightly less pronounced similarity is observed for a group of transverse-optic phonons with frequencies at $\simeq 4.5$ THz shown by a wider and less color-intense bulletlike trace in panel (a) and by a broad and structured peak in (c). Finally, a moderate doublet trace, the low-frequency bimodal peak in the multicolored curve in panel (c), corresponds to phonons with frequencies near the van Hove singularities at $\simeq 2.2$ and 2.7 THz for two transverse-acoustic branches [36], which also share some similarity in local vibrational motion with the BP modes. Panel (d) in Fig. 5 shows cross sections of $\mathcal{P}(\nu_g, \nu_c)$ along the horizontal lines in (a), corresponding to phonons with local dynamics similar to the BP modes. All of them exhibit relatively broad maxima near the BP frequency. Moreover, the crystallinity, a cumulative characteristic of the similarity of local vibrations in a glassy mode with any of the phonons, shows a peak [see Fig. 5(b)] remarkably coincident with the BP. This means that the BP modes exhibit the maximum similarity in local vibrations with phonons and, in fact, with optic phonons [cf. optic and acoustic contributions in Fig. 5(b)].

All models, v-SiO$_2$, lg-SiO$_2$, and pc-SiO$_2$, exhibit very similar correlation functions in the whole frequency range [cf. (a), (b), and (c) in Fig. 4] including the low-frequency domain $\lesssim 8$ THz [cf. panels (a), (e), and (f) in Fig. 5]. Both lg-SiO$_2$ and pc-SiO$_2$ models can be considered as toy models for silica glass which are created by using different types of disorder. The lg-SiO$_2$ model, by construction, preserves the network structure of perturbed tetrahedra, is free of topological disorder, and is globally anisotropic. In contrast, the pc-SiO$_2$ model consists of nonperturbed tetrahedra present in α-cristobalite but is globally isotropic. Our analysis demonstrates that the type of disorder introduced in a crystal does not play a significant role in the reconstruction of the phonon spectrum. Once disorder is introduced in a crystal, the spectrum transforms in a rather general way, such as band broadening and density tail formation, exhibiting very clear traces of the original spectrum where hybridization effects are not strong enough. These robust traces of phonons, e.g., with frequencies around 4.5 and 5.5 THz in the low-frequency range [see Figs. 5(a), 5(e) and 5(f)], are clearly seen for all models.

The three groups of phonons most similar to BP modes are characterized by the range of the wave vectors which are displayed in Fig. 6. In particular, the transverse-optic phonons with $\nu_c \simeq 4.5$ and 5.5 THz are characterized by wave-vector magnitude $q \simeq 0.15$–0.35 and 0.05–0.15 Å^{-1}, respectively, whereas the transverse-acoustic phonons from the low-frequency doublet at $\nu_c \simeq 2.2$ and 2.7 THz have $q \simeq 0.35$–0.45 Å^{-1}. These phonon wave-vector magnitudes are consistent with those of typical wave vectors of transverse plane waves $q \simeq 0.2$–0.5 Å^{-1}, contributing to the dynamical structure factor [37] in the BP range $\nu_g \sim 0.5$–2.5 THz (see Fig. S8 in the Supplemental Material [24]).

The strong similarity in local motion for BP modes and optic phonons near 5 THz can be explained as follows. The local projectional analysis for BP modes shows that these modes are mainly of F_1 symmetry for the T_d group (tetrahedral rotations) with the relative partial vibrational density of states reaching a maximum value of $\gtrsim 0.8$ near the BP (see Fig. 7). A similar analysis for phonons reveals that the maximum contribution from vibrations of the same F_1 symmetry is observed
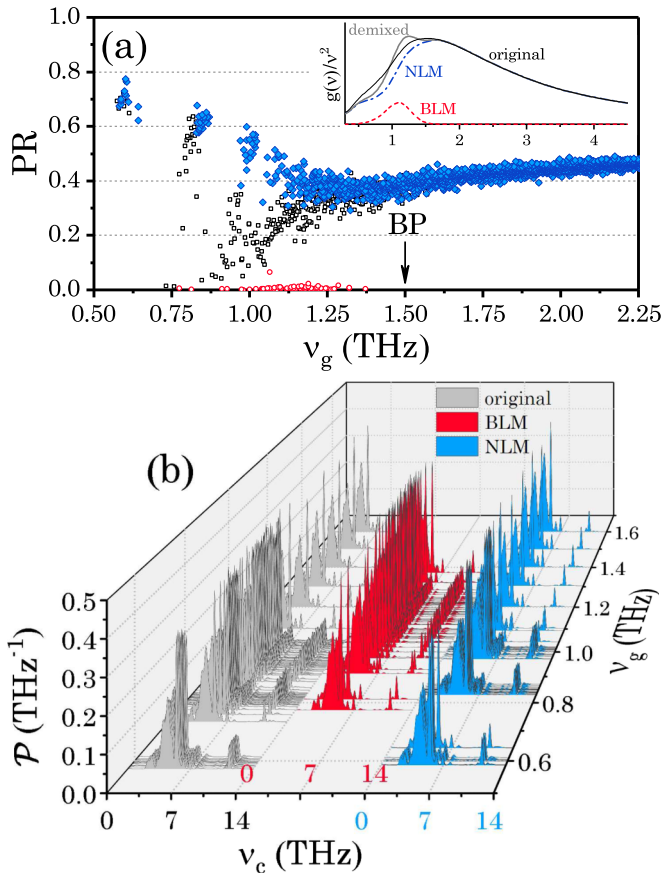
FIG. 9. (a) PR for glassy modes: original modes before demixing (empty black squares), nonlocalized plane-wave-like vibrational modes (NLMs) (filled blue diamonds), and bare localized modes (BLMs) (empty red circles) after demixing see the Supplemental Material [24] and Ref. [38]. The demixing parameters are $\Delta\nu/\nu = 0.3$ and $p_c = 0.25$ (see the Supplemental Material [24]). The inset shows the reduced VDOS for the original glassy modes (black curve), NLMs (dashed-dotted blue curve), and BLMs (dashed red curve) after demixing and the sum of BLMs and NLMs after demixing (solid gray curve). (b) Correlation function given by Eq. (6) for the original glassy modes, BLMs, and NLMs for projections onto the T_d group.

for optic phonons with frequencies near 5 THz with $0 \lesssim q \lesssim 0.5$ Å^{-1} (see Fig. 8) and, thus, not surprisingly, exactly these phonons are very similar to the BP modes. Therefore, the BP modes in v-SiO$_2$ can be locally described in terms of coupled tetrahedral rotations which mainly are very similar to those for transverse-optic phonons (cf. the qualitative picture given in Refs. [11,39,40]).

The vibrational modes found numerically at frequencies below the BP can be split into two types: (i) extended plane-wave-like states with PR $\gtrsim 0.5$, combined in discrete-frequency groups, characteristic of finite-size models; (ii) quasilocalized *optic* tail states with PR $\lesssim 0.4$ [see Fig. 9(a)]. The origin of the quasilocalized states and their possibly important role in determining the thermal conductivity are under active study [12,13,41]. The quasilocalized states can be considered as a mixture of NLMs and BLMs [38,42]. By applying a demixing technique [24,38], we separated the NLMs and BLMs [see Fig. 9(a)] and performed a comparative local symmetry-mode projectional analysis in order to reveal the phonon traces in these states. The results shown in Fig. 9(b) do not reveal any significant differences in local vibrational motion before and after demixing so that the dominant contributions in local motion (which is of F_1-rotation type) for both NLMs and BLMs come from groups of transverse-optic phonons at 4.5 and 5.5 THz similar to BP modes. This means that, even for the lowest-frequency ($\simeq 0.57$ THz for our finite-size model) plane-wave-like glassy modes, the local tetrahedral vibrations are similar to those for optic phonons with frequencies of 4.5 and 5.5 THz in α-cristobalite.

V. CONCLUSIONS

To conclude, a local symmetry-mode comparative projection technique has been developed and used for revealing *phonon traces* in glassy vibrational modes for all frequency ranges. In particular, strong optic-phonon traces are found for the BP modes and quasilocalized modes in the low-frequency range. The similarity in phonon traces discovered for glass, lattice-glass, and polycrystalline models with different types of disorder signify the presence of a common mechanism for the reconstruction of the phonon spectrum, independent of the type of disorder. The method described in the paper is general and can be applied to a broad class of monatomic and binary materials, e.g., Si, Ge, GeO$_2$, P$_2$O$_5$, GeSe$_2$, Si$_3$N$_4$, B$_2$O$_3$, Ta$_2$O$_5$, HfO$_2$, etc., in which local atomic triplets belonging to the C$_{2v}$ group, *A-A-A* or *A-B-A* are present [43].

[1] S. N. Taraskin and S. R. Elliott, Phonons in vitreous silica: dispersion and localization, Europhys. Lett. **39**, 37 (1997).

[2] W. Schirmacher, G. Diezemann, and C. Ganter, Harmonic Vibrational Excitations in Disordered Solids and the "Boson Peak", Phys. Rev. Lett. **81**, 136 (1998).

[3] S. N. Taraskin, Y. L. Loh, G. Natarajan, and S. R. Elliott, Origin of the Boson Peak in Systems with Lattice Disorder, Phys. Rev. Lett. **86**, 1255 (2001).

[4] V. M. Giordano and G. Monaco, Fingerprints of order and disorder on the high-frequency dynamics of liquids, Proc. Natl. Acad. Sci. USA **107**, 21985 (2010).

[5] G. Baldi, M. Zanatta, E. Gilioli, V. Milman, K. Refson, B. Wehinger, B. Winkler, A. Fontana, and G. Monaco, Emergence of Crystal-Like Atomic Dynamics in Glasses at the Nanometer Scale, Phys. Rev. Lett. **110**, 185503 (2013).

[6] M. Moratalla, J. F. Gebbia, M. A. Ramos, L. C. Pardo, S. Mukhopadhyay, S. Rudić, F. Fernandez-Alonso, F. J. Bermejo, and J. L. Tamarit, Emergence of glassy features in halomethane crystals, Phys. Rev. B **99**, 024301 (2019).

[7] A. A. Maradudin, The frequency shift and lifetime of a localized vibration mode, Ann. Phys. (NY) **30**, 371 (1964).

[8] R. J. Elliott, J. A. Krumhansl, and P. L. Leath, The theory and properties of randomly disordered crystals and related physical systems, Rev. Mod. Phys. **46**, 465 (1974).

[9] T. S. Grigera, V. Martin-Mayor, G. Parisi, and P. Verrocchio, Phonon interpretation of the "boson peak" in supercooled liquids, Nature (London) **422**, 289 (2003).

[10] A. I. Chumakov, G. Monaco, A. Fontana, A. Bosak, R. P. Hermann, D. Bessas, B. Wehinger, W. A. Crichton, M. Krisch, R. Rüffer, G. Baldi, G. Carini, Jr., G. Carini, G. D'Angelo, E. Gilioli, G. Tripodo, M. Zanatta, B. Winkler, V. Milman, K. Refson, M. T. Dove, N. Dubrovinskaia, L. Dubrovinsky, R. Keding, and Y. Z. Yue, Role of Disorder in the Thermodynamics and Atomic Dynamics of Glasses, Phys. Rev. Lett. **112**, 025502 (2014).

[11] U. Buchenau, N. Nücker, and A. J. Dianoux, Neutron Scattering Study of the Low-Frequency Vibrations in Vitreous Silica, Phys. Rev. Lett. **53**, 2316 (1984).

[12] U. Buchenau, Y. M. Galperin, V. L. Gurevich, and H. R. Schober, Anharmonic potentials and vibrational localization in glasses, Phys. Rev. B **43**, 5039 (1991).

[13] V. L. Gurevich, D. A. Parshin, and H. R. Schober, Anharmonicity, vibrational instability, and the boson peak in glasses, Phys. Rev. B **67**, 094203 (2003).

[14] W. Schirmacher, G. Ruocco, and T. Scopigno, Acoustic Attenuation in Glasses and Its Relation with the Boson Peak, Phys. Rev. Lett. **98**, 025501 (2007).

[15] A. Giuntoli and D. Leporini, Boson Peak Decouples from Elasticity in Glasses with Low Connectivity, Phys. Rev. Lett. **121**, 185502 (2018).

[16] M. Baggioli and A. Zaccone, Universal Origin of Boson Peak Vibrational Anomalies in Ordered Crystals and in Amorphous Materials, Phys. Rev. Lett. **122**, 145501 (2019).

[17] J. Yang, Y.-J. Wang, E. Ma, A. Zaccone, L. H. Dai, and M. Q. Jiang, Structural Parameter of Orientational Order to Predict the Boson Vibrational Anomaly in Glasses, Phys. Rev. Lett. **122**, 015501 (2019).

[18] S. N. Taraskin, Connection between structural characteristics of glasses and their crystalline counterparts, J. Phys.: Condens. Matter **19**, 455215 (2007).

[19] A. I. Chumakov, G. Monaco, A. Monaco, W. A. Crichton, A. Bosak, R. Rüffer, A. Meyer, F. Kargl, L. Comez, D. Fioretto, H. Giefers, S. Roitsch, G. Wortmann, M. H. Manghnani, A. Hushur, Q. Williams, J. Balogh, K. Parliński, P. Jochym, and P. Piekarz, Equivalence of the Boson Peak in Glasses to the Transverse Acoustic Van Hove Singularity in Crystals, Phys. Rev. Lett. **106**, 225501 (2011).

[20] S. Plimpton, Fast parallel algorithms for short-range molecular dynamics, J. Comput. Phys. **117**, 1 (1995).

[21] B. W. H. van Beest, G. J. Kramer, and R. A. van Santen, Force Fields for Silicas and Aluminophosphates Based on *ab initio* Calculations, Phys. Rev. Lett. **64**, 1955 (1990).

[22] A. Carré, L. Berthier, J. Horbach, S. Ispas, and W. Kob, Amorphous silica modeled with truncated and screened Coulomb interactions: A molecular dynamics simulation study, J. Chem. Phys. **127**, 114512 (2007).

[23] N. S. Shcheblanov, B. Mantisi, P. Umari, and A. Tanguy, Detailed analysis of plastic shear in the Raman spectra of SiO_2 glass, J. Non-Cryst. Solids **428**, 6 (2015).

[24] See Supplemental Material at http://link.aps.org/supplemental/10.1103/PhysRevB.102.024202 for details on generation of models, local projection analysis, phonon dispersion in α-cristobalite, dynamical structure factor and mode demixing procedure.

[25] K. Mizokami, A. Togo, and I. Tanaka, Lattice thermal conductivities of two SiO_2 polymorphs by first-principles calculations and the phonon Boltzmann transport equation, Phys. Rev. B **97**, 224306 (2018).

[26] R. T. Downs and D. C. Palmer, The pressure behavior of α-cristobalite, Am. Min. **79**, 9 (1994).

[27] A. F. Wright and A. J. Leadbetter, The structures of the β-cristobalite phases of SiO_2 and $AlPO_4$, Philos. Mag. **31**, 1391 (1975).

[28] H. Tanaka, H. Tong, R. Shi, and J. Russo, Revealing key structural features hidden in liquids and glasses, Nat. Rev. Phys. **1**, 333 (2019).

[29] P. Hirel, Atomsk: A tool for manipulating and converting atomic data files, Comput. Phys. Commun. **197**, 212 (2015).

[30] S. N. Taraskin and S. R. Elliott, Nature of vibrational excitations in vitreous silica, Phys. Rev. B **56**, 8605 (1997).

[31] N. S. Shcheblanov, M. E. Povarnitsyn, S. N. Taraskin, and S. R. Elliott, Addendum and Erratum: Nature of vibrational excitations in vitreous silica [Phys. Rev. B 56, 8605 (1997)]; Phys. Rev. B **94**, 099903(E) (2016).

[32] S. N. Taraskin and S. R. Elliott, Disorder-induced zero-energy spectral singularity for random matrices with correlations, Phys. Rev. B **65**, 052201 (2002).

[33] M. Wilson, P. A. Madden, M. Hemmati, and C. A. Angell, Polarization Effects, Network Dynamics, and the Infrared Spectrum of Amorphous SiO_2, Phys. Rev. Lett. **77**, 4023 (1996).

[34] J. Sarnthein, A. Pasquarello, and R. Car, Origin of the high-frequency doublet in the vibrational spectrum of vitreous SiO_2, Science **275**, 1925 (1997).

[35] J. J. Ludlam, S. N. Taraskin, S. R. Elliott, and D. A. Drabold, Universal features of localized eigenstates in disordered systems, J. Phys.: Condens. Matter **17**, L321 (2005).

[36] The assignment of the predominant polarization (transverse or longitudinal) for acoustic and optic phonons is based on an analysis of phonon dispersion and the dynamical structure factor (see Figs. S5, S7, and S8 in the Supplemental Material [24]).

[37] S. N. Taraskin and S. R. Elliott, Connection between the true vibrational density of states and that derived from inelastic neutron scattering, Phys. Rev. B **55**, 117 (1997).

[38] H. R. Schober and C. Oligschleger, Low-frequency vibrations in a model glass, Phys. Rev. B **53**, 11469 (1996).

[39] J. C. Phillips, T^3 specific-heat anomaly in network solids, Phys. Rev. B **32**, 5356 (1985).

[40] B. Hehlen, E. Courtens, R. Vacher, A. Yamanaka, M. Kataoka, and K. Inoue, Hyper-Raman Scattering Observation of the

Boson Peak in Vitreous Silica, Phys. Rev. Lett. **84**, 5355 (2000).

[41] L. Wang, A. Ninarello, P. Guan, L. Berthier, G. Szamel, and E. Flenner, Low-frequency vibrational modes of stable glasses, Nat. Commun. **10**, 26 (2019).

[42] S. N. Taraskin and S. R. Elliott, Anharmonicity and localization of atomic vibrations in vitreous silica, Phys. Rev. B **59**, 8572 (1999).

[43] A. S. Barker and A. J. Sievers, Optical studies of the vibrational properties of disordered solids, Rev. Mod. Phys. **47**, S1 (1975).